Chinese Chemical Letters 34 (2023) 107370

Contents lists available at ScienceDirect

Chinese Chemical Letters

journal homepage: www.elsevier.com/locate/cclet

SiO_2 nanofiber composite gel polymer electrolyte by *in-situ* polymerization for stable Li metal batteries

Zhichuan Shen[1], Jiawei Zhong[1], Jiahong Chen, Wenhao Xie, Kun Yang, Yuhan Lin, Jinbiao Chen, Zhicong Shi*

School of Materials and Energy, Guangdong University of Technology, Guangzhou 510006, China

ARTICLE INFO

Article history:
Received 10 January 2022
Revised 26 February 2022
Accepted 23 March 2022
Available online 25 March 2022

Keywords:
SiO_2 nanofiber
In-situ polymerization
Composite gel polymer electrolytes
1,3-Dioxolane
Lithium metal-LFP battery

ABSTRACT

Gel polymer electrolytes (GPEs) are promising alternatives to liquid electrolytes applied in high-energy-density batteries. Here superior SiO_2 nanofiber composite gel polymer electrolytes (SNCGPEs) are developed *via in-situ* ionic ring-opening polymerization of 1,3-dioxolane (DOL) monomers in SiO_2 nanofiber membrane (PDOL-SiO_2) for lithium metal batteries. The oxygen atoms of PDOL together with Si-O of SiO_2 construct a more efficient channel for Li^+ migration. Consequently, the lithium ion transference number (t_{Li^+}) and ionic conductivity (σ) at 30 °C of PDOL-SiO_2 are 0.80 and 1.68×10^{-4} S/cm separately. PDOL-SiO_2 manifests the electrochemical decomposition potentials of 4.90 V. At 0.5 mA/cm^2, Li|PDOL-SiO_2|Li cell shows a steady cycling performance for nearly 1400 h. LFP|PDOL-SiO_2|Li battery can steadily cycle at 0.5 C with a capacity retention rate of 89% after 200 cycles. While cycling at 2 C, the capacity retention rate can maintain at 78% after 300 cycles. This contribution provides a innovative strategy for accelerating Li^+ transportation *via* designing PDOL molecular chains throughout the SiO_2 nanofiber framework, which is crucial for high-energy-density LMBs.

Lithium metal batteries (LMBs) have attracted much attention due to its high theoretical specific capacity (3860 mAh/g) [1,2]. Unfortunately, safety hazards generating from the uncontrollable interfacial reactions between liquid electrolytes (LEs) and high energy electrodes still hinder the practical application of LMBs [3].

Considering this situation, replacing LEs with gel polymer electrolytes (GPEs) will efficaciously improve the cycling performance and safety of LMBs. GPEs generally consist of polymer network and small organic molecules, which present good physical properties to resist volume deformation of electrodes [4,5]. Even so, traditional strategies applied to prepare GPEs are attributable to *ex-situ* preparation methods, resulting in the low lithium-ion transference number and poor interfacial contact [6–8]. Accordingly, researchers have proposed the *in-situ* polymerization of GPEs to ameliorate these problems. This methodology can effectively bridge an integrated interface between the electrode particles and GPEs, thus deliberately enhancing the interfacial conformability [9]. During a routine procedure, a precursor solution including initiators, monomers, and LEs are primarily injected into the cell package. After effectively wetting the active materials, a certain external condition is took to initiate polymerization inside the battery, thus crafting steady conformal interfaces [10].

Although the advantages of *in-situ* polymerization are obvious, most previous *in-situ* polymerization components are initiators and non-electrolytic monomers, which is not easily implementable under moderate external conditions [11]. Therefore, a facile preparation method for *in-situ* GPEs must be developed to meet the practical requirements. Among all the candidate monomers, 1,3-dioxolane (DOL) is able to form poly(1,3-dioxolane) (PDOL) *via* ionic ring-opening polymerization, which can be initiated by most of the Lewis acids [12]. It is believed that the electrochemical reduction products generated from PDOL forms passivate interphases on Li anode to prevent continuous degradation of GPEs, enabling highly reversible charge-discharge performance [13]. Nevertheless, the non-crosslinked structure of obtained PDOL is unable to supply sufficient mechanical properties to inhibit the volume deformation of electrodes [14]. Actually, this problem can be ameliorated by adding inorganic nano fillers into the GPEs.

Silicon dioxide (SiO_2) nanofibers have been proved to enhance the thermal stability, mechanical strength, and electrochemical performances of GPEs [15,16]. With the incorporation of SiO_2 nanoparticles, the pathways are created to transport Li^+ through constructing the interactions between SiO_2 surface and anions [17]. However, this transportation path is inconsecutive, which means

* Correspondng author.
E-mail address: zhicong@gdut.edu.cn (Z. Shi).
[1] These authors contributed equally to this work

https://doi.org/10.1016/j.cclet.2022.03.093
1001-8417/

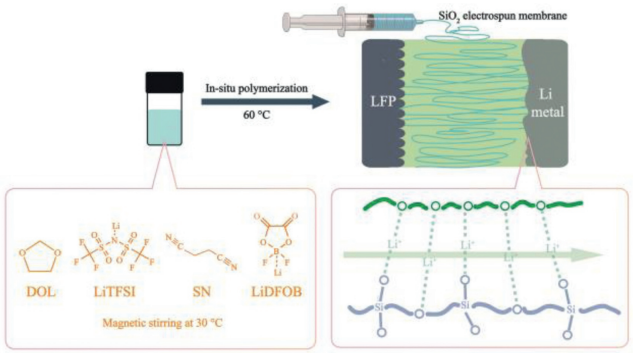

Scheme 1. Fabrication process of *in-situ* polymer electrolytes (PDOL-SiO_2).

that a connected Li^+ transfer network cannot be built, owing to the isolation distribution characteristics of nanoparticles [18]. Thus, the effect of enhancing Li^+ mobility is reduced. Considering this situation, because of the highly efficient in synthesizing the nanofibers with high porosity and favourable flexibility, electrospinning technique can be applied to transform SiO_2 into a unique 3D nanofiber frame [19]. Such 3D reinforced architecture *via* incorporating GPEs into a SiO_2 spinning membrane will take effect as an enhancement strategy for interfacial Li^+ transport channel. Even so, less reports focus on the combination between 3D SiO_2 nanofiber frame and *in-situ* SNCGPEs.

In this study, DOL is infiltrated into the SiO_2 porous membrane to fabricate PDOL *via* the process of *in-situ* ionic ring-opening polymerization (Scheme 1). The oxygen atoms of PDOL together with Si-O of SiO_2 construct a more efficient channel for Li^+ migration. Consequently, the t_{Li^+} and σ at 30 °C of PDOL-SiO_2 are separately 0.80 and 1.68×10^{-4} S/cm. PDOL-SiO_2 manifests the electrochemical decomposition potentials of 4.90 V. At 0.5 mA/cm^2, Li|PDOL-SiO_2|Li cell shows a steady cycling performance for nearly 1400 h. LFP|PDOL-SiO_2|Li battery can cycle steadily at 0.5 C at 30 °C, keeping a capacity retention rate of 89% after 200 cycles. Even at 2 C, the capacity retention rate can maintain at 78% after 300 cycles. It is obvious that SiO_2 spinning membrane makes PDOL perform a better property in LMBs than that of PE membrane. This contribution provides a innovative strategy for accelerating Li^+ transportation *via* designing PDOL molecular chains throughout the SiO_2 membrane, which is crucial for high-energy-density LMBs.

For preparing SiO_2 nanofiber membrane, the stable and homogenous tetraethyl orthosilicate (TEOS) and poly(vinyl alcohol) (PVA) solutions (TEOS:PVA = 8:1) were fabricated using a conventional electrospinning parameters (Voltage: 20 kV; air gap distance: 15 cm; inner diameter of spinneret: 0.4 mm; flow rate of solution: 1 mL/h). The optimal concentration of the PVA/TEOS solution was 11% w/w. In addition, the experiment was conducted consistently at 25 °C in the air. Finally, SiO_2 membrane were calcinated for 8 h at 800 °C in air to take away the residual PVA. In the process of *in situ* preparation of PDOL-SiO_2, about 2 mol/L LiTFSI and 0.3 mol/L LiDFOB were added into a mixed solution of DOL reagent with 30 wt% SN and completely dissolved at 30 °C with continuous stirring for 1 h. About 200 μL of the precursor solution was injected into a SiO_2 membrane and then assembled into the cells. The assembled cells were aged for 120 min to make sure that the electrodes were well-wetted with the precursor solution. Subsequently, heating at 60 °C for 12 h would make the DOL completely polymerize into PDOL. For comparison, polyethylene (PE) membrane was applied to combine with the precursor solution in the same way. The other information including chemical materials, preparation of $LiFePO_4$ (LFP) cathodes, materials characterization, and electrochemical measurements were provided in supporting information.

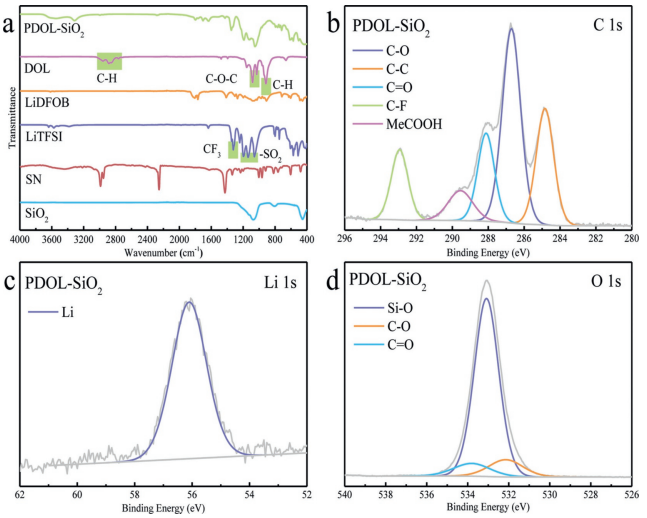

Fig. 1. (a) Fourier infrared spectrometer (FTIR) spectra of materials at 4000~400 cm^{-1}. X-ray photoelectron spectroscopy (XPS) spectra on (b) C 1s, (c) Li 1s and (d) O 1s of PDOL-SiO_2.

The morphologies of SiO_2 membrane and PDOL-SiO_2 were observed by SEM. Obviously, SiO_2 membrane presents a porous structure composed of nanowires with a diameter of about 200 nm (Figs. S1a and b in Supporting information), which will assist in adsorbing precursor solutions and maximizing the t_{Li^+} of PDOL-SiO_2 after ionic ring-opening polymerization [20]. In Figs. S1c and d (Supporting information), after the *in-situ* ionic ring-opening polymerization, SiO_2 membrane manifests a wrinkly surface, meaning that the entire SiO_2 support are full of PDOL. As expected, thermal polymerization reaction make PDOL-SiO_2 form a high compatibility interface to act as Li^+-conductive path [21]. Figs. S2a–e (Supporting information) illustrate the digital photographs of flexural strength of SiO_2 membrane, clearly demonstrating that the SiO_2 membrane has good bending resistance, which is beneficial to support the PDOL. In Figs. S2g (Supporting information), it is clearly that liquid precursor solution translate into a transparent gel when compared with that in Figs. S2f (Supporting information), indicating that DOL monomers polymerize into the large molecules.

FTIR was took to verify the chemical groups evolution of PDOL-SiO_2 (Fig. 1a). For DOL, the peaks located at 1029 cm^{-1} and 1081 cm^{-1} are attributed to the C-O-C structure, while peak at 915 cm^{-1} is ascribed to the C-H out of plane vibration [22]. Compared with DOL, the PDOL-SiO_2 displays an obvious displacement in the C-O-C vibration and the disappearance of the C-H out-of-plane vibration, suggesting that the DOL monomers are bound together by ionic ring-opening polymerization [23]. This also confirms the macroscopic phenomenon observed in Figs. S1 (Supporting information). Moreover, the peaks belong to -CF_3 and -SO_2 structures are observed in the range of 1000~1400 cm^{-1} in spectral line of PDOL-SiO_2, which mean the successful addition of lithium salt. For SN, the peak located at 2254 cm^{-1} is attributable to nitrile group, while the added PDOL decreases the intensity of this peak owing to the interaction between PDOL and SN [24].

XRD patterns of SiO_2, PE, PDOL-SiO_2, and PDOL-PE are also showed in Figs. S3a and b (Supporting information). PE shows two sharp peaks from 20° to 25°, which validate that PE membrane presents the crystal structure [25]. In the case of PDOL-PE, the above peaks can still be observed, which indicates the maintainence of crystal structure with the introduction of PDOL. Although the appropriate crystallinity will be beneficial to the stability of mechanical properties, the crystal phase is not only inconducive to the Li^+ transportation, but also increased the

impedance of the electrolyte [26]. On the contrary, only a broad peak at about 21° is seen in both the pattern of PDOL-SiO_2 and SiO_2, confirming the amorphous phase of electrospun SiO_2 fibrous membrane and PDOL-SiO_2. The amorphous phase is able to capture more polymeric pecursor solution and form a closer relationship between supporting membrane and PDOL, which is crucial for transporting Li^+. Thus, the amorphous characteristics will make PDOL-SiO_2 manifest a better Li^+ transportation than that of PDOL-PE.

TGA measurement was used to examine the decomposition process of PDOL-SiO_2 (Fig. S3c in Supporting information). For SiO_2, a negligible weight loss in the range of 30~800 °C is showed in the curves, indicating that this membrane displays a excellent thermostable performance. The polymerization leads to a improvement of the stability up to 100 °C for PDOL, while PDOL-SiO_2 makes a gradual weight loss in the range of the same temperature, which may be due to the elimination of moisture [27,28]. Both of them exhibit the weight loss start from 400 °C, being attributed to the decomposition of LiTFSI [29]. Because of the addition of SN, the additional mass drop in the range of 150~300 °C is also observed in TGA curves PDOL and PDOL-SiO_2 [30]. Specially, compared to PDOL, the weight before 450 °C of PDOL-SiO_2 reduces more slowly, which mean that the application of SiO_2 membrane is beneficial for improving the temperature resistance of PDOL.

DSC measurement was employed to examine the physical properties of PDOL-SiO_2. For comparison, PE membrane is also applied as a support for PDOL. Fig. S3d (Supporting information) displays the DSC curves of PDOL-SiO_2 and PDOL-PE. The T_g of PDOL-PE is at around -8 °C and no endothermic peak can be observed, which demonstrated that PDOL-PE exits in amorphous state due to the absence of further transitions above T_g [31]. In contrast, no thermodynamic transition behavior can be observed in curves of PDOL-SiO_2, indicating that PDOL-SiO_2 remains the amorphous state within the test temperature range. Thus, PDOL-SiO_2 possesses the improved segmental motion in the networks of SiO_2 with a wider range of adaptive temperatures, which may bring the higher t_{Li^+} [32,33].

To investigate the chemical change in the materials, XPS was applied to analyze the PDOL-SiO_2 and SiO_2 membrane (Figs. 1b–d). In the C 1s and O 1s spectra of PDOL-SiO_2, the C-C (284.84 eV) and C-O (286.71 eV and 532.14 eV) peaks are assigned to the molecular chains of PDOL. In addition, C=O (288.12 eV and 533.80 eV) and MeCOO- (289.55 eV) peaks belonged to ester structures of LiDFOB also appear, while the observation of C-F peak (292.94 eV) is ascribed to the addition of LiTFSI and LiDFOB. For Li 1s, peak at 56.10 eV can be assigned to the Li^+ of LiTFSI and LiDFOB. Thus, FTIR spectroscopy together with XPS analysis confirm the successful fabrication of PDOL-SiO_2. Generally, the binding energy (BE) of peak shift positively mean the electrons transfer among different atoms [34]. Thus, when compared with Si-O peak (533.01 eV) of SiO_2 in Fig. S3e (Supporting information), that peak of PDOL-SiO_2 in Fig. 1d shift positively to 533.08 eV. Such positive shift proves the coordination between Li^+ and oxygen atoms of SiO_2, indicating that the SiO_2 membrane is also involved in the transportation of Li^+.

Fig. S4 (Supporting information) and Fig. 2a show the EIS and σ of the PDOL-SiO_2 and PDOL-PE in the temperature range from 0 to 90 °C. The σ at 30 °C of PDOL-SiO_2 is 1.68×10^{-4} S/cm, higher than that of PDOL-PE (1.43×10^{-5} S/cm). A higher σ is indicative of the faster ionic migration, which will improve the charge-discharge performance of batteries at room temperature. Furthermore, as an significant parameter, the t_{Li^+} is employed to evaluate the Li^+ transport efficiency of lithium batteries (LMBs) (Fig. 2b). t_{Li^+} for PDOL-SiO_2 is 0.80 at 30 °C, which is larger than that of GPEs in recent reports (Fig. S5 in Supporting information). The large t_{Li^+} will reduce concentration polarization and shows a positive effect on the charge-discharge capacity of batteries, as the low t_{Li^+} will cause concentration gradients in electrolytes and finally leads to a premature failure of batteries [35]. The high σ and t_{Li^+} together confirm the vital function of SiO_2 membrane in accelerating the Li^+ transportation as analyzed above.

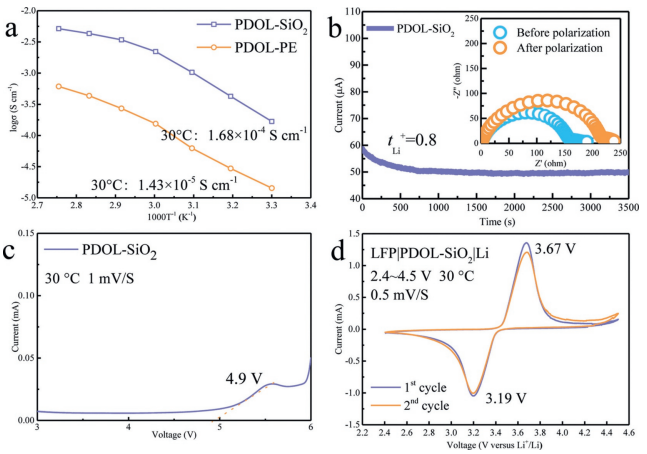

Fig. 2. (a) Temperature-dependent ionic conductivity for PDOL-SiO_2 and PDOL-PE. (b) Chronoamperometry profiles and AC impedance spectra of lithium symmetric cell with PDOL-SiO_2 before and after polarization. (c) LSV curves of PDOL-SiO_2 at 3.0~6.0 V. (d) CV curves of LFP|PDOL-SiO_2|Li battery at 2.4~4.5 V.

LSV was applied to obtain the appropriate electrochemical window of the electrolyte for the following cycling investigation (Fig. 2c). It shows that the decomposition potentials of PDOL-SiO_2 at 30 °C is about 4.9 V, which is much higher than that of PEO (3.8 V). The high oxidative resistance of inorganic ceramic material mainly accounts for this result [36].

To evaluate the cathode compatibility of PDOL-SiO_2, LMBs of LFP|PDOL-SiO_2|Li were measured at 30 °C by different methods. CV curves of LFP|PDOL-SiO_2|Li are shown in Fig. 2d. The oxidation-reduction process of Fe^{2+}/Fe^{3+} of LFP|PDOL-SiO_2|Li displays a couple of redox peaks in the CV curves, which is related to extracting/embedding process of Li^+ [37]. All samples exhibit conspicuous overlaps and small potential differences due to the favourable ionic conductivity, which represents the enhancement of electrochemical reversibility [38].

The cycling performance of batteries using PDOL-SiO_2 or PDOL-PE as electrolyte were investigated at 30 °C. The LFP|PDOL-PE|Li battery can only keep a capacity retention rate of 56% after 60 cycles at 0.5 C (Fig. S6a in Supporting information). More seriously, when under a constant current of 1 C, the capacity retention rate will decrease to 50% after 100 cycles (Fig. S6b in Supporting information). By contrast, LFP|PDOL-SiO_2|Li presents a capacity retention rate of 89% after 200 cycles at 0.5 C, while that is 89% after 100 cycles under a constant current of 1 C, which corresponds to discharge capacities of 120.11 and 114.89 mAh/g, respectively (Figs. 3a and b, Figs. S7a and b in Supporting information).

The rate performances of LFP|PDOL-SiO_2|Li and LFP|PDOL-PE|Li were also investigated at 30 °C from 2.4 V to 4.2 V (Fig. 3c and Fig. S6c in Supporting information). The discharge specific capacity of LFP|PDOL-SiO_2|Li at the currents of 0.5 C, 1 C and 2 C are 137.4, 115.7 and 93 mAh/g, respectively (Fig. S7c in Supporting information), which are higher than those of LFP|PDOL-PE|Li. LFP|PDOL-SiO_2|Li presents a better discharge specific capacity than that of LFP|PDOL-PE|Li either at low or at high rates, which is attributed to the faster Li^+ transportation resulting from the construction of fast ion channel between SiO_2 and PDOL. Based on this, LFP|PDOL-SiO_2|Li cycling at 2 C are also investigated at 30 °C. PDOL-SiO_2 makes LFP operate stably for 300 cycles under a constant current of 2 C with the discharge capacity and capacity retention rate of

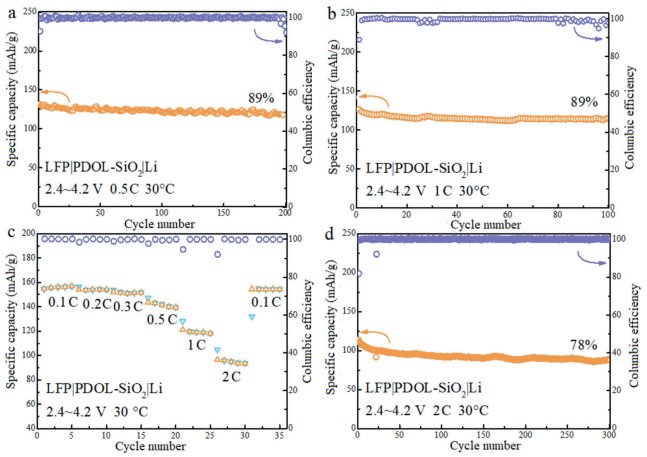

Fig. 3. Cycling performance of LFP|PDOL-SiO_2|Li batteries at (a) 0.5 C, (b) 1 C, (c) various current densities and (d) 2 C at 30 °C.

88 mAh/g and 78%, respectively (Fig. 3d and Fig. S7d in Supporting information).

To understand the cycling behaviors of LFP|PDOL-SiO_2|Li and LFP|PDOL-PE|Li, the EIS of the above batteries recorded before cycling was compared with that at 100th cycle (Fig. S8 in Supporting information). The R_0 at high frequency represents ohmic resistance of lithium battery, while R_1 is the interface impedance between lithium anode and GPEs [39]. Moreover, the R_2 of LFP-GPEs interface impedance at intermediate-frequency and the Li^+ diffusion in LFP cathodes presented by a low-frequency tail are also observed in EIS curves before cycling and after 100 cycles [39]. With the assist of Zview software, the variation of fitted resistance of LFP|PDOL-SiO_2|Li and LFP|PDOL-PE|Li before cycling and after 100 cycles are showed in Fig. S9 (Supporting information). After cycling at 30 °C, the R_0 of LFP|PDOL-SiO_2|Li and LFP|PDOL-PE|Li increase from 8.04 and 5.58 Ω to 26.87 and 27.03 Ω, respectively, indicating that the lithium metal changes structurally during charge-discharge process. In addition, R_1 and R_2 of LFP|PDOL-SiO_2|Li change from 2.06 and 128.40 Ω to 231.20 and 50.32 Ω, respectively, while those of LFP|PDOL-PE|Li change from 138.00 and 207.70 Ω to 39.88 and 774.60 Ω, respectively, which is attributed to the interface variation during cycling [35]. Obviously, LFP|PDOL-SiO_2|Li performs the smaller increase of R_2 than that of LFP|PDOL-PE|Li, indicating that application of SiO_2 porous membrane makes PDOL more stable with LFP in the charge-discharge process than that of PE. However, the value of R_1 of LFP|PDOL-SiO_2|Li increases, while that of LFP|PDOL-PE|Li decrease, indicating that compatibility of PDOL-PE with lithium anode is better than that of PDOL-SiO_2, which needs the further research in the future.

The lithium plating and stripping processes of Li|PDOL-SiO_2|Li battery were evaluated at 30 °C (Fig. S10 in Supporting information). Li metal anode of the Li|PDOL-SiO_2|Li cell can cycle stably for nearly 1000 h with an overpotential of less than 50 mV at a current density of 0.5 mA/cm^2, which indicatives that Li|PDOL-SiO_2|Li cell has a small resistance and a decreased polarization of the SEI film. The high t_{Li^+} conduces to facilitate a uniform deposition and stripping of Li^+ at the electrode/electrolyte interface, which may explain the above phenomenon [40]. However, compared with the recent reference, the stable cycling time of this system in lithium symmetric battery is shorter [41]. The difference is mainly caused by the different polymer applied in the batteries with different molecular chain structures. Introduction of some rigid structure, such as the phenyl structure in OP-10, may offer the electrolyte better resistance to lithium dendrite growth when compared with the pure ether structure.

In summary, DOL is successfully infiltrated into the SiO_2 porous membrane to fabricate PDOL *via* the *in-situ* ionic ring-opening polymerization process. PDOL-SiO_2 presents a better thermal stability than that of LEs. The oxygen atoms of PDOL together with Si-O of SiO_2 construct a more efficient Li^+ migration channel. On account of this, the t_{Li^+} and σ at 30 °C of PDOL-SiO_2 are enhanced to 0.80 and 1.68×10^{-4} S/cm, respectively. PDOL-SiO_2 manifests the electrochemical decomposition potentials of 4.90 V. At 0.5 mA/cm^2, Li|PDOL-SiO_2|Li cell shows a much more steady cycling performance for nearly 1400 h. Noticeably, LFP|PDOL-SiO_2|Li battery cycled at 0.5 C at 30 °C shows a capacity retention rate of 89% after 200 cycles. Even at 2 C, the capacity retention rate can maintain at 78% after 300 cycles. SiO_2 membrane based PDOL performs a better property in LMBs than that of PE membrane. This study provides an innovative strategy for accelerating Li^+ transportation *via* designing PDOL molecular chains throughout the SiO_2 membrane, which is crucial for high performance LMBs.

Declaration of competing interest

The authors declare that they have no known competing financial interests or personal relationships that could have appeared to influence the work reported in this paper.

Acknowledgments

This work is supported by the Department of Science and Technology of Zhuhai City (No. ZH22017001200059PWC) and the Department of Science and Technology of Guangdong Province, China (No. 2019A050510043).

Supplementary materials

Supplementary material associated with this article can be found, in the online version, at doi:10.1016/j.cclet.2022.03.093.

References

[1] J.R. Nair, L. Imholt, G. Brunklaus, et al., Electrochem. Soc. Interface 28 (2019) 55–61.
[2] Y. Zhang, T. Zuo, J. Popovic, et al., Mater. Today 33 (2020) 56–74.
[3] L. Liu, J. Lyu, J. Mo, et al., Sci. China Mater. 63 (2020) 703–718.
[4] W. Ren, C. Ding, X. Fu, et al., Energy Storage Mater. 34 (2021) 515–535.
[5] Z. Hu, G. Li, A. Wang, et al., Batter. Supercaps 3 (2020) 331–335.
[6] W.D. Richards, L.J. Miara, Y. Wang, et al., Chem. Mater. 28 (2016) 266–273.
[7] W. Tang, S. Tang, C. Zhang, et al., Adv. Energy Mater. 8 (2018) 1800866.
[8] Z. Lin, X. Guo, H. Yu, Nano Energy 41 (2017) 646–653.
[9] Y. Cho, C. Hwang, D.S. Cheong, et al., Adv. Mater. 31 (2019) 1804909.
[10] T. Liu, J. Zhang, W. Han, et al., J. Electrochem. Soc. 167 (2020) 70527.
[11] V. Vijayakumar, B. Anothumakkool, S. Kurungot, et al., Energ. Environ. Sci. 14 (2021) 2708–2788.
[12] C. Zhao, Q. Zhao, X. Liu, et al., Adv. Mater. 32 (2020) 1905629.
[13] Q. Zhao, X. Liu, J. Zheng, et al., Proc. Nat. Acad. Sci. U. S. A. 117 (2020) 26053.
[14] H. Yang, M. Jing, H. Li, et al., Chem. Eng. J. 421 (2020) 129710.
[15] D. Lin, W. Liu, Y. Liu, et al., Nano Lett. 16 (2016) 459–465.
[16] P. Yang, X. Gao, X. Tian, et al., ACS Energy Lett. 5 (2020) 1681–1688.
[17] Y. Lin, Y. Chen, S. Hou, et al., J. Mater. Chem. A 5 (2017) 17476–17481.
[18] Z. Shen, Y. Cheng, S. Sun, et al., Carbon Energy 3 (2021) 482–508.
[19] M. Wang, Y. Wu, M. Qiu, et al., J. Energy Chem. 61 (2021) 253–268.
[20] C. Fu, Y. Ma, P. Zuo, et al., J. Power Sour. 496 (2021) 229861.
[21] J. Wu, Z. Rao, Z. Cheng, et al., Adv. Energy Mater. 9 (2019) 1902767.
[22] T. Chen, H. Wu, J. Wan, et al., J. Energy Chem. 62 (2021) 172–178.
[23] Q. Liu, B. Cai, S. Li, et al., J. Mater. Chem. A 8 (2020) 7197–7204.
[24] B.N. Nadirah, C.C. Ong, M.S.M. Saheed, et al., Int. J. Hydrog. Energy 45 (2020) 19590–19600.
[25] A. Aattache, R. Soltani, A. Mahi, Constr. Build. Mater. 146 (2017) 603–614.
[26] Y. Zhao, L. Wang, Y. Zhou, et al., Adv. Sci. 8 (2021) 2003675.
[27] S. Almuhamed, M. Bonne, N. Khenoussi, et al., J. Ind. Eng. Chem. 35 (2016) 146–152.
[28] İ. Gergin, E. Ismar, A.S. Sarac, Beilstein J. Nanotech. 8 (2017) 1616–1628.
[29] Z. Lu, L. Yang, Y. Guo, J. Power Sour. 156 (2006) 555–559.
[30] K. Liu, Q. Zhang, B.P. Thapaliya, et al., Solid State Ion. 345 (2020) 115159.
[31] C. Wang, H. Zhang, S. Dong, et al., Chem. Mater. 32 (2020) 9167–9175.
[32] L. Yu, Y. Zhang, J. Wang, et al., Macromolecules 54 (2021) 874–887.

[33] Y. Yao, Z. Wei, H. Wang, et al., Adv. Energy Mater. 10 (2020) 1903698.
[34] Z. Shen, H. Wen, H. Zhou, et al., Mater. Sci. Eng. C 105 (2019) 110073.
[35] Z. Shen, J. Zhong, W. Xie, et al., Acta Metall. Sin. 34 (2021) 359–372.
[36] S. Tang, W. Guo, Y. Fu, Adv. Energy Mater. 11 (2021) 2000802.
[37] Q. Cheng, X. Zhao, G. Yang, et al., Energy Storage Mater. 41 (2021) 842–882.
[38] S. Yang, Q. Fan, Z. Shi, et al., ACS Appl. Mater. Interfaces 11 (2019) 36742–36750.
[39] H. Yamauchi, J. Ikejiri, K. Tsunoda, et al., Sci. Rep. 10 (2020) 9453.
[40] C. Ma, K. Dai, H. Hou, et al., Adv. Sci. 5 (2018) 1700996.
[41] C. Sun, J. Dong, X. Lu, et al., Adv. Funct. Mater. 31 (2021) 2100594.